Formation of Superheavy Elements and Ternary Fission Fragment Mass Distribution

V. Yu. Denisov[*,a,b]

[a]*Gesellschaft für Schwerionenforschung mbH, Planckstr. 1, Darmstadt, 64291, Germany*
[b]*Institute for Nuclear Research, Prospect Nauki 47, Kiev 03650, Ukraine*

The cold fusion reactions related to ^{208}Pb and ^{209}Bi targets leading to superheavy elements with $Z = 104$–112 have been successfully considered in our model recently. Here we briefly discuss this model and extend our consideration to another type of fusion reactions. The interaction potential between heavy ions around the touching point is calculated for various Skyrme forces in the extended Thomas-Fermi approximation by using the frozen Hartree-Fock-Bogoliubov densities of the individual nuclei. The shape of fragment mass distribution in the case of ternary fission mode is discussed in detail.

1. Introduction

We shortly discuss three different items of nuclear reactions with participation of very heavy nuclei. The first item is connected with the superheavy elements (SHEs) production in heavy-ions fusion reaction. The second one is related with the properties of the ion-ion interaction potential between very heavy nuclei, because the properties of the ion-ion interaction potential are very important for the SHE production cross section. The third item is devoted to the particularities of ternary fission mode in heavy actinides. These items are considered below in corresponding sections.

2. Formation of SHEs in Nucleus-Nucleus Collision

The synthesis of superheavy elements was and still is an outstanding research object. The properties of SHEs are studied both theoretically and experimentally.[1,2] In the cold fusion, SHEs are produced by reactions of the type X + (Pb, Bi) → SHE + 1n at subbarrier energies.[1] The excitation energy of a compound nucleus formed by cold fusion is low, $\approx$10–20 MeV.[1] The experimental study of an excitation function for the SHE production becomes increasingly difficult due to very small cross sections and narrow width of the excitation function.[1]

In Reference 2 we present a model for description of measured excitation functions for the SHE production in cold fusion reactions. The maximum position and the width of the excitation function for cold fusion reactions X + ^{208}Pb,^{209}Bi leading to elements with $Z = 104$–112 are well described in Reference 2 (see also Figure 1). Within our approach[2] the process of the SHE formation proceeds in three stages: (*i*) The capture of two spherical nuclei and the formation of a common shape of the two touching nuclei. Low-energy surface vibrations and a transfer of few nucleons are taken into account at the first step of the reaction. (*ii*) The formation of a spherical or near spherical compound nucleus. (*iii*) The surviving of an excited compound nucleus during evaporation of neutrons and γ-ray emission which compete with fission. A reduction of the fission barrier is taken into account, which arises from a reduction of the shell effects at increasing excitation energy of the compound nucleus.

One of the heaviest systems experimentally studied over a wider range of excitation energy is ^{64}Ni + ^{208}Pb → ^{271}110 + n,[1] the data are shown in Figure 1. The experimental data are compared with several modifications of our model. In the simplest case, using tunneling through a one-dimensional barrier and the WKB method, the model strongly underestimates the experimental fusion cross sections. Better agreement is obtained, when the neutron transfer channels from lead to iron are taken into account. Similarly, the cross sections increase if the low-energy 2^+ and 3^- surface vibrational excitations

of both projectile and target are included in the calculations, see Figure 1. The best fits are obtained by considering transfer and vibrations simultaneously. The values of parameters and other details are presented in Reference 2. In our model[2] we have two fitting parameters as well as other parameters, which are taken from experimental data and from other calculations, see Reference 2 for detail. Note that we are able to describe data for reactions ^{62}Ni + ^{208}Pb → ^{269}110 + n (see Figure 1) and ^{64}Ni + ^{209}Bi → ^{272}111 + n (see figure 12 in Reference 2) by using the same fitting parameters as fixed for reaction ^{64}Ni + ^{208}Pb → ^{271}Hs + n.

The results of similar calculations for reaction ^{54}Cr + ^{208}Pb → ^{261}Sg + n are also presented in Figure 1. Our calculation well agrees with the experimental data.

Reactions with targets slightly lighter than Pb are also interesting for studying too. The reactions between ^{76}Ge + ^{198}Pt → ^{273}110 + n, ^{82}Se + ^{192}Os → ^{273}110 + n, ^{76}Ge + ^{186}W → ^{261}Sg + n, and ^{82}Se + ^{180}Hf → ^{261}Sg + n are compared[3] with the cold fusion reactions leading to the same SHE in Figure 1. Reactions with ^{76}Ge and ^{82}Se projectiles in Figure 1 are strongly enhanced by coupling to both neutron transfer and low-energy surface vibrations. More symmetric reactions with ^{82}Se projectile have smaller difference between the capture barrier height and the ground state Q-value energy of compound nucleus formed at fusion. Due to this, the SHE production cross sections for reactions with Se projectile are higher than the one for Ge, see Figure 1. Note that it would be interesting to check experimentally our estimates for both symmetric reactions and reactions with ^{76}Ge and ^{82}Se projectiles considered in Figure 1.

3. Potential Between Heavy Ions

Knowledge of the ion-ion interaction potential is a key ingredient in the analysis of nuclear reactions. By using the potential between nuclei, we can estimate the cross sections of different nuclear reactions.[4] The ion-ion interaction potential related to the Coulomb repulsion force and the nuclear attraction force has, as a rule, the barrier and the capture potential well near a touching point. The Coulomb part of the ion-ion potential is well-known. In contrast, the nuclear part of the nucleus-nucleus potential is less defined. There are many different approaches to the nuclear part of the interaction potential.[4–8] Unfortunately, barriers evaluated within different approaches for the same colliding system differ considerably, especially when both nuclei are very heavy or one nucleus is very heavy and another is light. The uncertainty of the interaction potential between heavy ions near the touching point gives rise to a variety of proposed nuclear reaction mechanisms. The uncertainty of the interaction potential between heavy ions became extremely large in reactions used for the production of superheavy elements. So, there is a need to reduce the uncertainty of the interaction potential

*E-mail: v.denisov@gsi.de; denisov@kinr.kiev.ua.
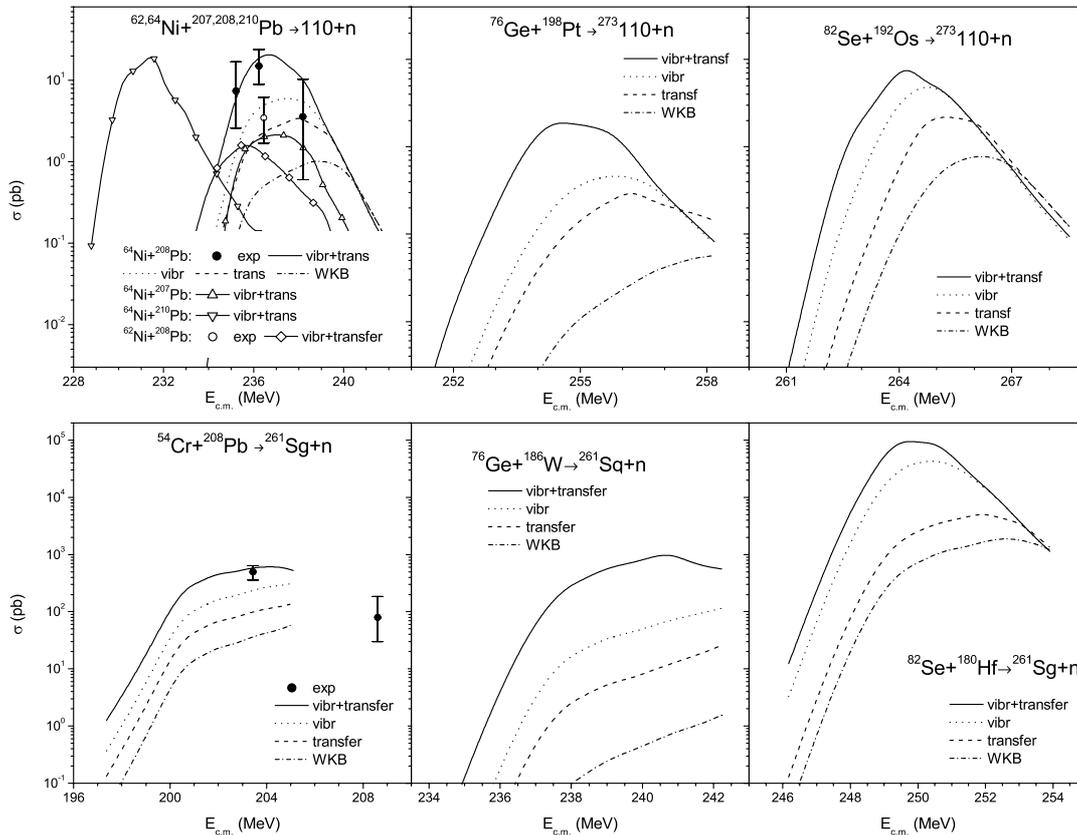
Figure 1. Calculated excitation functions for the reactions $^{62,64}Ni + {}^{207,208,210}Pb \rightarrow 110 + n$ (upper left panel), $^{76}Ge + {}^{198}Pt \rightarrow {}^{273}110 + n$ (upper middle panel), $^{82}Se + {}^{192}Os \rightarrow {}^{273}110 + n$ (upper right panel), $^{54}Cr + {}^{208}Pb \rightarrow {}^{261}Sg + n$ (bottom left panel), $^{76}Ge + {}^{186}W \rightarrow {}^{261}Sg + n$ (bottom middle panel), and $^{82}Se + {}^{180}Hf \rightarrow {}^{273}Sg + n$ (bottom right panel). The solid curves take into account both the low-energy 2^+ and 3^- (only for reactions with Pb, see also text) vibrations and the neutrons transfer channels. The dotted and the dashed curves for these reactions show the results based on solely the 2^+ and 3^- (only for reactions with Pb, see also text) vibrations and the neutron transfer channels, respectively. The results of the one-dimensional WKB approach for these reactions are shown by the dash-dotted curves. The experimental data are taken from Reference 1.

around the touching point.

The interaction energy between ions is obtained with the help of a local energy density functional. The extended Thomas-Fermi (ETF) approximation with $\hbar^2$ correction terms is used for the evaluation of the kinetic energy density functional.[10] The Skyrme[10] and Coulomb energy density functionals are em-

ployed for the calculation of the potential energy. These energy density functionals depend on the proton and neutron densities. These densities are obtained in the microscopic Hartree-Fock-Bogoliubov approximation with the Skyrme force. Our approximation is semi-microscopic because we use the microscopic density distributions and the ETF approximation for the calculation of the interaction energy of ions. The details of our calculation is presented in Reference 9.

In Figure 2, we present the interaction potentials between ^{70}Zr and ^{208}Pb evaluated in the ETF approximation with different parameter sets of the Skyrme force.[10] The potentials obtained by using different analytical expressions[4-7] are also shown in Figure 2. The ion-ion potentials obtained for SkM*, SkP, and SLy4 sets are very close to each other at all distances presented in Figure 2. The potential wells obtained in the ETF approximation are shallow. The minimal value of the potential well is located at the distance smaller than the touching point distance of two spherical ions, which is close to 12 fm. Here we roughly determined touching point distance as $R = r_0(A_1^{1/3} + A_2^{1/3})$, where $r_0 = 1.2$ fm. Therefore both processes, the capture of two ions and the neck formation, take place in the potential well.

The barriers obtained with the help of different analytical expressions for ion-ion potential[4-7] are spread in very wide interval in Figure 2. The Krappe-Nix-Sierk (KNS) potential[6] is the most closest to the ETF potentials.

The interaction potentials evaluated in the ETF approximation between various combinations of both spherical nuclei or spherical and deformed nuclei are presented in Reference 9.

4. Ternary Fission Fragment Mass Distribution

The binary fission fragment mass distribution has been studied in various nuclei.[11] Unfortunately, the ternary fission fragment mass distribution has not been studied in detail. There is
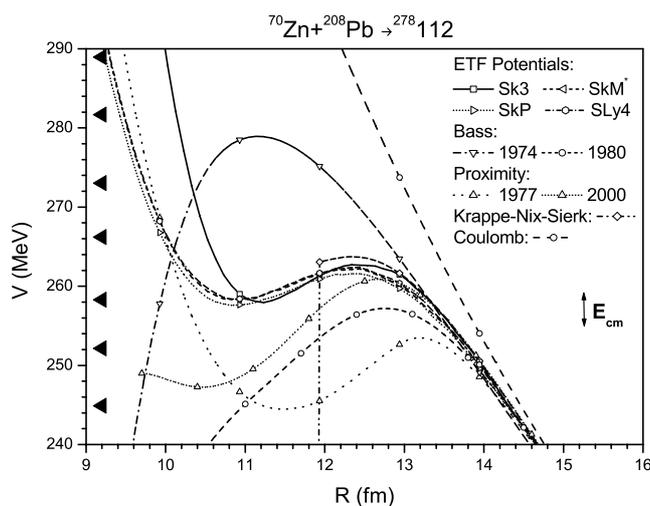
Figure 2. The potentials for the collision $^{70}Zr + {}^{208}Pb$ evaluated in the ETF approximation with Sk3, SkM*, SkP, and SLy4 parameter sets of the Skyrme force. The Coulomb potential and the potentials obtained in the two versions (1974 and 1980 years) of the Bass parametrization, in the KNS parametrization and in two versions of proximity approximation (1977 and 2000 years) are also presented. The range of collision energies in the middle of the target used in experiments[1] is marked by vertical arrow in the right part. The ground state fusion reaction Q-values are marked by lowest triangle in the left side. The other upper 6 triangles in the left part are related with $1n$, $2n$, $3n$, $4n$, $5n$, and $6n$ separation energies respectively.
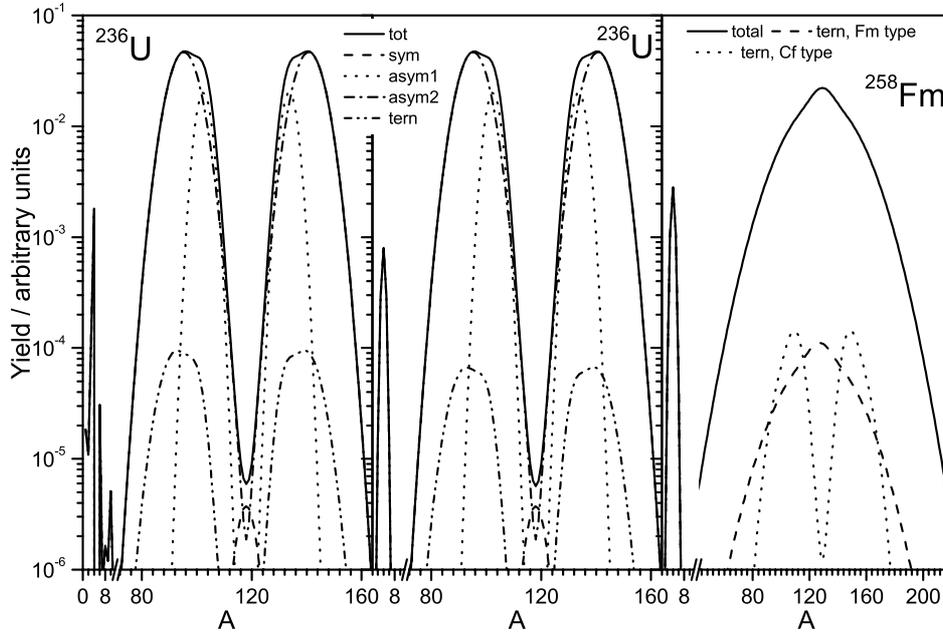
Figure 3. The total and ternary fission fragment mass distributions of ^{236}U (left and middle panels) and ^{258}Fm (right panel). The partial contributions of symmetric (sym), two asymmetric (asym1 and asym2), and ternary (tern) fission modes are shown in the case of ^{236}U. The total and ternary fission fragment mass distributions of ^{258}Fm are presented in the case of two different assumptions of the ternary fission fragment mass formation process, see text for details.

only few data on the ternary fission fragment mass distribution obtained in coincidence with α particle in several nuclei.[11–14] Below we study in detail the shape of ternary fission fragment mass distribution.

For the sake of more general consideration, we propose that a nucleus decays by three binary fission modes accompanied by ternary fission modes. The three binary fission modes are associated with symmetric and two different asymmetric fission modes. Distributions of the fragment mass for the binary fission modes can be described in the multimodal approach[15] as

$$Y_s(A) = g(A, A_0/2, \sigma_s), \qquad (1)$$

$$Y_{ai}(A) = g(A, A_{ai}, \sigma_{ai}) + g(A, A_0 - A_{ai}, \sigma_{ai}). \qquad (2)$$

Here $g(a,b,\sigma) = \exp[-((a-b)/\sigma)^2]/(\sqrt{\pi}\sigma)$, σ_s, σ_{ai} are the widths of corresponding distributions, $i = 1, 2$, A_0 is the number of nucleons in nucleus, A_{ai} is the number of nucleons in fragment, related with the position of maximal yield of corresponding asymmetric fission mode.

The nucleus decay into two heavy fragments and light particle during the ternary fission.[11–14] The mass distribution of the light particle emitted at ternary fission is localized near $A_{LP} = 4$ (Ref. 11–14)

$$y_{lp}(A_{lp}) = g(A_{lp}, A_{LP}, \sigma_{lp}), \qquad (3)$$

where σ_{lp} is the width of distribution. The total yields of both fission fragments should correlate with the yields of light particles. The ternary fission fragment mass distribution is, as a rule, similar to the binary fission fragment mass distribution.[13,14,16] Therefore, we consider three heavy fragment ternary fission modes associated with corresponding symmetric and two asymmetric binary fission modes. Note that the maximums of ternary fission fragment mass distributions are shifted to the smaller values of A due to the light particle emission. For the case of asymmetric ternary fission mode, these shifts may be different for light and heavy maximums of the fragment mass distribution.[13,14,16] So, we can describe the ternary fission fragment mass distribution accompanied by emission of light particle with A_{lp} nucleons as

$$y_{st}(A, A_{lp}) = g(A, (A_0 - A_{lp})/2, \sigma_{st}) y_{lp}(A_{lp}), \qquad (4)$$

$$y_{ati}(A, A_{lp}) = [g(A, A_{ai} - p_i A_{lp}, \sigma_{ati})$$
$$+ g(A, A_0 - A_{ai} - (1 - p_i)A_{lp}, \sigma_{ati})] y_{lp}(A_{lp}), (5)$$

where $\sigma_{st}, \sigma_{ati}$ are the widths of corresponding distributions, $p_i A_{lp}$ and $(1 - p_i)A_{lp}$ are the shifts of light and heavy maximums of the fission fragment mass distribution due to the light particle emission A_{lp}. By means of eq 3–5, we obtain the total two-dimensional ternary fission fragment mass distribution in the form

$$Y_{ti}(A, A_{lp}) = y_{lp}(A_{lp}) + w_{st}y_{st}(A, A_{lp})$$
$$+ w_{at1}y_{at1}(A, A_{lp}) + w_{at2}y_{at2}(A, A_{lp}). \qquad (6)$$

Here w_{st}, w_{at1}, and w_{at2} are the weights of corresponding ternary fission modes, $w_{st} + w_{at1} + w_{at2} = 1$.

The experimental data on the fragment mass distribution are associated, as a rule, with an one-dimensional distribution.[11] Therefore, we transform the two-dimensional ternary fission fragment mass distribution into the one-dimensional one. The yield of fission fragment with mass A at ternary fission is

$$Y_t(A) = y_{lp}(A) + \sum_{A_{lp}} [w_{st}y_{st}(A, A_{lp})$$
$$+ w_{at1}y_{at1}(A, A_{lp}) + w_{at2}y_{at2}(A, A_{lp})]. \qquad (7)$$

This fragment mass distribution is asymmetric with respect to $A_0/2$.

The total fragment mass distribution is a sum of the yields of different fission modes with corresponding weights

$$Y_{tot}(A) = w_s Y_s(A) + w_{a1}Y_{a1}(A) + w_{a2}Y_{a2}(A) + w_t Y_t(A), \qquad (8)$$

where $w_s + w_{a1} + w_{a2} + w_t = 1$.

Let us study the shape dependence of the initial total one-dimensional fission fragment mass distribution on the properties of ternary fission mode. The total fission fragment mass distribution and partial contribution of each fission mode are shown in Figure 3. In the case of fission ^{236}U, we perform calculation for $A_0 = 236$, $A_{a1} = 102.36$, $A_{a2} = 95.24$, $\sigma_s = 4.243$, $\sigma_{a1} = 3.649$, $\sigma_{a2} = 6.916$, $w_{a1} = 0.092814$, $w_{a2} = 0.405687$, $w_s = 0.000998$, $w_{at1} = 0.093$, $w_{at2} = 0.4065$, $w_{st} = 0.001$, $w_t = 0.002$. The values of parameters $A_{a1}, A_{a2}, \sigma_s, \sigma_{a1}$, and σ_{a2} are the same as obtained in Reference 17 for the low-energy neutron induced fission of ^{235}U. However, we slightly changed the relative yields of binary fission modes from that obtained in Reference 17, because the ternary fission contribution was neglected in this reference. Due

to the similarity of binary and ternary fission fragment mass distributions of ^{236}U (Ref. 13, 16), we use for the weights w_{ati} and w_{st} exactly the same values as in Reference 17 for corresponding binary modes, and put $\sigma_{ati} = \sigma_{ai}$ and $\sigma_{st} = \sigma_s$. But the final width of ternary fission fragment mass distribution for the each mode is slightly larger than the width of corresponding binary fission mode, because of the convolution of two distributions in eq 4, 5. We choose $p_i = 0.7$ (Ref. 18) according to the experimental observation of ternary fragment mass distribution of ^{236}U (Ref. 13, 16).

The experimental light particle mass distribution from Reference 14 is substituted as $y_{lp}(A_{lp})$ in left panel of Figure 3. In middle panel of Figure 3 the light particle mass distribution is modulated by eq 3 with $A_{LP} = 4$ and $\sigma_{lp} = 1$. By comparing left and middle panels in Figure 3 we cannot see visible changes of the shapes of both total and ternary fission fragment mass distributions. In contrast to this the light particle mass distributions presented in the left and middle panels of Figure 3 are drastically changed.

The total ternary fission fragment mass distribution is mainly related with the ternary fission accompanied by α particle. The characteristics of ternary fission fragment mass distribution may be connected with the fission properties of both the initial nucleus and nucleus formed by removing α particle from the initial nucleus. The ternary fission fragment mass distribution is very similar to the binary fission fragment mass distribution in ^{236}U, because the characteristics of fission modes in ^{236}U and ^{232}Th are similar.[15]

It is interesting to know which nucleus, initial or nucleus formed by removing α particle from the initial nucleus, play the most important role in the formation of ternary fission fragment mass distribution. It is possible to clear up this question by studying the ternary fission fragment mass distribution in ^{258}Fm, because the binary fission fragment mass distribution of ^{258}Fm and ^{254}Cf are, respectively, symmetric and asymmetric.[19, 20]

In the right panel of Figure 3, we present the results of our simulation of total, binary, and ternary fission fragment mass distribution of ^{258}Fm. Firstly, we propose that the ternary fission fragment mass distribution of ^{258}Fm is determinated by the fission properties of the initial nucleus ^{258}Fm. In this case, the ternary fission fragment mass distribution is symmetric and similar to the binary fragment mass distribution of ^{258}Fm. We equate the corresponding widths of ternary and binary fission fragment mass distributions and put $p_i = 0.5$ in calculation. The parameters of fragment mass distribution for ^{258}Fm are obtained by fitting the data for reactions ^{257}Fm(n_{th}, f).[19] Secondly, we guess that the ternary fission fragment mass distribution of ^{258}Fm is determinated by the fission properties of ^{254}Cf. The shapes of ternary and binary fragment mass distributions of ^{258}Fm are very different, because the ternary fission fragment mass distribution is asymmetric in this case. The parameters of fragment mass distribution of ^{254}Cf are evaluated by fitting the data for reactions ^{254}Cf(sf).[20] Probably, the realistic ternary fission fragment mass distribution is a superposition of the both fragment mass

formation modes. It is very interesting to check experimentally which mode is more important for the ternary fission fragment mass formation process.

References

(1) S. Hofmann and G. Münzenberg, Rev. Mod. Phys. **72**, 733 (2000).

(2) V. Yu. Denisov and S. Hofmann, Phys. Rev. C **61**, 034606 (2000).

(3) Note that our code is proposed for the evaluation of the SHE production cross section in fusion of two spherical nuclei.[2] However we may simulate static deformation effect in deformed target by taking the same value of the vibration 2^+ amplitude as the value of static quadrupole deformation. We equate the energy of the first 2^+ vibration state to the value of 1st rotational 2^+ state in deformed nuclei.

(4) R. Bass, *Nuclear Reactions with Heavy Ions* (Springer-Verlag, Berlin, 1980).

(5) J. Blocki, J. Randrup, W. J. Swiatecki, and C. F. Tang, Ann. Phys. **105**, 427 (1977).

(6) H. J. Krappe, J. R. Nix, and A. J. Sierk, Phys. Rev. C **20**, 992 (1979).

(7) W. D. Myers and W. J. Swiatecki, Phys. Rev. C **62**, 044610 (2000).

(8) A. Winther, Nucl. Phys. A **594**, 203 (1995).

(9) V. Yu. Denisov and W. Nörenberg (in preparation).

(10) M. Brack, C. Guet, and H.-B. Hakanson, Phys. Rep. **123**, 275 (1985).

(11) R. Vandenbosch and J.R. Huizenga, *Nuclear Fission* (Academic Press, New York, 1973).

(12) I. Halpern, Ann. Rev. Nucl. Sci, **21**, 245 (1971).

(13) C. Wagemans, *Particle Emission from Nuclei, vol. 3*, edited by D. N. Poenaru and M. S. Ivascu (CRC Press, Inc., Boca Raton, 1989), p. 63.

(14) M. Mutterer and J. P. Theobald, *Nuclear Decay Modes*, edited by D. N. Poenaru (IOP, Bristol, 1996), p. 487.

(15) U. Brosa, S. Grossmann, and A. Müller, Phys. Rep. **197**, 167 (1990); U. Brosa, H.-H. Knitter, T.-S. Fan, J.-M. Hu, and S.-L. Bao, Phys. Rev. C **59**, 767 (1999).

(16) R. K. Choudhury, S. S. Kapoor, D. M. Nadkani, and P. N. Rama Rao, Nucl. Phys. A **346**, 473 (1980).

(17) Ch. Straede, C. Budtz-Jorgensen, and H.-H. Knitter, Nucl. Phys. A **462**, 85 (1987).

(18) This value of p is related with the fact that the distribution of light fragments is shifted to the lower value of mass more than the distribution of heavy fragments.[16]

(19) W. John, E. K. Hulet, R. W. Lougheed, and J. J. Wesolowski, Phys. Rev. Lett. **27**, 45 (1971).

(20) J. Gindler, Phys. Rev. C **19**, 1806 (1979).